Taylor & Francis
Taylor & Francis Group

Fullerenes, Nanotubes and Carbon Nanostructures

ISSN: (Print) (Online) Journal homepage: www.tandfonline.com/journals/lfnn20

Determining the defect type in a graphene lattice

Margaret Archibald, Sonja Currie & Marlena Nowaczyk

To cite this article: Margaret Archibald, Sonja Currie & Marlena Nowaczyk (2024) Determining the defect type in a graphene lattice, Fullerenes, Nanotubes and Carbon Nanostructures, 32:4, 311-317, DOI: 10.1080/1536383X.2023.2280752

To link to this article: https://doi.org/10.1080/1536383X.2023.2280752

Published online: 14 Nov 2023.

Submit your article to this journal

Article views: 128

View related articles

View Crossmark data

Citing articles: 1 View citing articles

Full Terms & Conditions of access and use can be found at
https://www.tandfonline.com/action/journalInformation?journalCode=lfnn20

FULLERENES, NANOTUBES AND CARBON NANOSTRUCTURES
2024, VOL. 32, NO. 4, 311–317
https://doi.org/10.1080/1536383X.2023.2280752

Taylor & Francis
Taylor & Francis Group

Check for updates

Determining the defect type in a graphene lattice

Margaret Archibald[a], Sonja Currie[a], and Marlena Nowaczyk[b,c]

[a]The John Knopfmacher Centre for Applicable Analysis and Number Theory, School of Mathematics, University of the Witwatersrand, Johannesburg, South Africa; [b]Faculty of Applied Mathematics, AGH University of Krakow, Krakow, Poland; [c]School of Information Technology, Halmstad University, Halmstad, Sweden

ABSTRACT

We consider four common defects that appear in an infinite single-layer graphene lattice, i.e. single vacancy $V_1(5-9)$, Stone-Wales SW $(55-77)$, and double vacancies $V_2(5-8-5)$ and $V_2(555-777)$. Investigating the honeycomb pattern of the graphene, we make use of the concept of shortest closed paths (periodic orbits) in the underlying topological structure. Using properties of the shortest closed paths of odd length we present and prove mathematically an algorithm that classifies which one of these defects occurs.

ARTICLE HISTORY
Received 7 September 2023
Accepted 27 October 2023

KEYWORDS
Graphene; inverse problem; single vacancy defect; double vacancy defect; Stone-Wales

MATHEMATICS SUBJECT CLASSIFICATION (2020)
47N60; 81Q10; 34A55; 34B45

1. Introduction

In recent years graphene has attracted a lot of attention from a wide variety of scientists, due to the single-layer honeycomb lattice structure which enables vast applications in nanotechnologies. Initially it was thought that defects made graphene less useful, but there is research emerging showing that certain defects can alter the properties (predominantly electronic, but also chemical, mechanical, thermal, optical, magnetic, etc.) in a beneficial way.

In some cases, defects arise naturally in the growth or processing of graphene, and in other cases, defects can be deliberately created to obtain specific properties. For instance, an electronic device or application which is difficult to switch off (due to the absence of a semiconducting gap in defect-free graphene) could be improved by introducing a suitable defect which has the potential of creating such a gap, see.[1]

The most common breaks observed experimentally are a single vacancy defect $V_1(5-9)$, a $V_2(5-8-5)$ double vacancy defect, a Stone-Wales (rotational) defect SW $(55-77)$, and a $V_2(555-777)$ double vacancy defect. From a geometrical point of view, single vacancies (SVs) are the simplest defects. They occur when one lattice atom is missing and a dangling bond always remains. Experimentally this has been observed by, for example,.[2,3] Double vacancies (DVs) occur when there are two lattice atoms missing and since an even number of missing atoms allows a full reconstruction (no dangling bonds), such vacancies are energetically and thermodynamically favoured over structures with an odd number of missing atoms where an open bond remains.[4] In some instances (depending on the structures) one DV defect can be more stable than another, see for example,[5] where $V_2(5-8-5)$ and $V_2(555-777)$ are compared. Even without adding or removing atoms, such as with the Stone-Wales (SW) defect where one edge/bond is rotated by 90 degrees, the structure of graphene can be changed significantly, affecting the properties. For related contributions in the field of the Stone-Wales rotation and use of the topological potential method we refer the reader to.[6–9]

Substantial electronic impacts of defects in graphene are discussed in.[1] Graphene's outstanding thermal conductivity makes it useful in thermal management applications, particularly high-power microelectronic devices, see.[10] Studies on the effects of topological defects on mechanical and physical properties of graphene are discussed in.[11] Additional theoretical results on the topology of carbon surfaces and related molecular objects, relevant to our studies on graphene lattices, are presented in[12,13] amongst others.

By considering graphene nanoribbons as quantum wires, the electron scattering can be modelled by a scattering matrix, see[14–16] amongst others. This matrix includes information from the transition and reflection matrices and it connects the amplitudes of scattered (outgoing) waves with the amplitudes of the incident (incoming) waves. The properties of a scattering matrix are changed in the presence of defects.

CONTACT Sonja Currie sonja.currie@wits.ac.za The John Knopfmacher Centre for Applicable Analysis and Number Theory, School of Mathematics, University of the Witwatersrand, Johannesburg, South Africa.

© 2023 Taylor & Francis Group, LLC

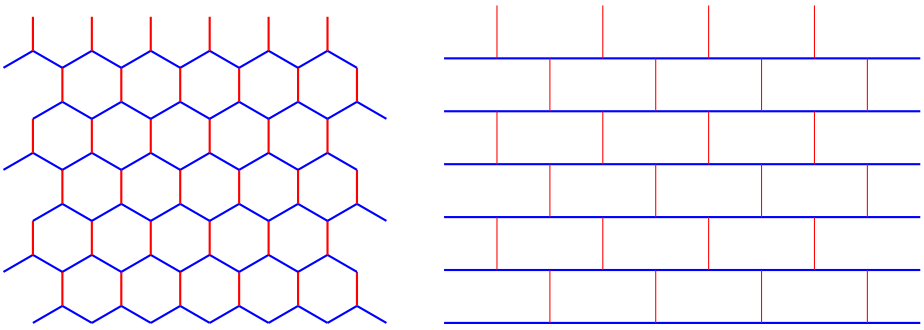

Figure 1. An infinite boundless hexagonal grid (left) with the corresponding brick wall representation (right).

Recently, in,[17–19] we investigated an infinite 3-regular hexagonal grid which models a graphene nano-ribbon (GNR). The carbon atoms are represented by the vertices and the bonds by edges each of length one. Low-energy free electrons "move" in this structure obeying the Laplace equation with so-called natural (Kirchhoff) boundary conditions at the vertices. In the 3-regular hexagonal grid, a closed path (periodic orbit) of odd length will occur only if a polygon with an odd number of sides is formed due to a defect. The presence of a periodic orbit of odd length enables us to determine the exact location, within the grid, of the defect.

By sending an electronic signal from one of the vertices and detecting the returning impulses, in theory, one could observe the spectrum of this structure. Using this approach, we are able to determine the lengths of all closed paths (periodic orbits) starting and ending at the given vertex where the detector is placed.

In order to reference the infinite single-layer hexagonal grid in terms of a coordinate system, our method in[17–19] was to transform the hexagonal grid to a rectangular grid resembling a brick wall and thus impose an (x, y)-coordinate system. A similar topological approach was used in.[20] This distortion is a compression in the vertical direction causing the non-vertical lines to become horizontal, as shown in Figure 1.

Since different defects affect the properties of graphene differently, it would be beneficial to classify the defect in the nano-ribbon structure. In this paper the following inverse problem is solved: If one of the four defects listed above occurs in the graphene, can we determine which one it is?

2. Properties of the regions

We begin by analysing the properties of the rectangular grid structure for the four different types of breaks. The grid is divided into different regions based on the properties of the closed paths of odd length. Let S be the length of the shortest closed path of odd length starting and ending at a reference point R. If R is at the top of a vertical line then:

- R lies in region A if and only if $S \equiv 1(\mathrm{mod}4)$,
- R lies in region B if and only if $S \equiv 3(\mathrm{mod}4)$.

Analogously, if R is at the bottom of a vertical line:

- R lies in region A if and only if $S \equiv 3(\mathrm{mod}4)$,
- R lies in region B if and only if $S \equiv 1(\mathrm{mod}4)$.

For the proof of these statements, see.[17] As a consequence, for the breaks shown in Figure 2 we obtain the arrangement of the regions in the rectangular grid as given in Figure 3 (see[17–19]) and will now note some important features of the regions that will be used in the motivation of the algorithm.

All the grids have a large upper wedge-shaped region (bounded by 45-degree boundaries) containing a top-central sub-region (TCSR) with darker shading, see Figure 4. This sub-region starts one unit above the centre of the upper boundary of a break and has boundaries which go up at 45-degree angles to the right and left. It is only in the SV break that this sub-region is an A region.

The dominating bottom-left sub-region (BLSR) is again a wedge (see Figure 4). The upper boundary of the BLSR lies on the horizontal line which runs through the lower pentagon and the lower boundary is defined by a 45-degree line originating from within the left-most pentagon of the break. Of the three breaks that have a B region for the TCSR, it is only for the SW break that the BLSR is an A region.

The bottom-central sub-region (BCSR) and the bottom-right sub-region (BRSR) are relevant for distinguishing between the two double vacancy breaks. For the BCSR, each grid has a similar-shaped A region directly below the break, where the two 45-degree lines originate from within the bottom pentagon. The BRSR in each case originates in the lower pentagon and is bounded by a horizontal line and a 45-degree line which begins from within the bottom pentagon as shown in Figure 4.

Note that, the minimal horizontal distance from the BLSR to the BRSR differs according to the number of regions between them. The more regions between, the longer the distance. I.e., the horizontal distance from the BLSR to the BRSR for $V_2(555-777)$ is two bricks longer (see the two diagonal white stripes in Figure 4) than for the $V_2(5-8-5)$ break.

3. Algorithm and motivation

In this section we will present an algorithm for determining which one of the four breaks occurs in the brick structure and consequently in the hexagonal graphene grid. We then prove the relevant steps rigorously in Lemma 3.2, Lemma 3.4 and Lemma 3.5.

In the algorithm below in order to determine in which region the detector is placed, one needs to use the statements in the bullet points in Section 2.

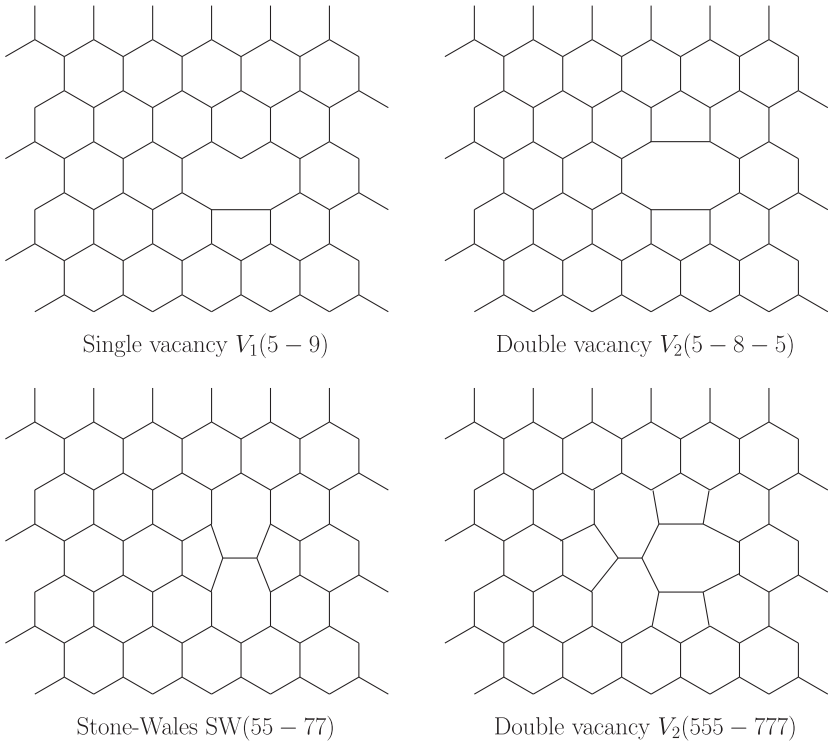

Figure 2. The four most common defects in the hexagonal grid.

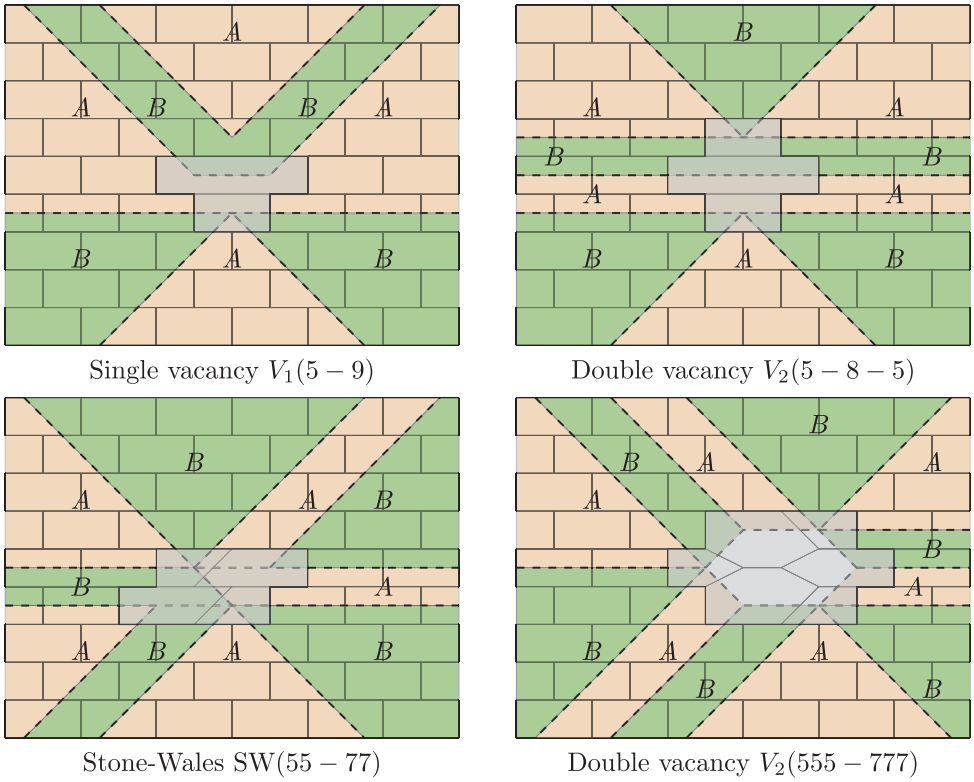

Figure 3. The regions for the four breaks.

Algorithm 3.1.

1. *Obtain a value for S1 by placing the detector at R1, which is any reference point at the top of a vertical line, and finding the value of the shortest closed path of odd length.*
2. *Move the detector vertically up by* $2S1$ *units to reach R2 - which will be at the top of a vertical line - and read the value of S2. If* $S2 \equiv 1(\mathrm{mod}4)$ *then R2 is in region A and the defect is a single vacancy, see Lemma 3.2.*
3. *If it is not a single vacancy (i.e., R2 is in region B), move the detector vertically down from R1 by* $\frac{S1+1}{2}$ *units and*

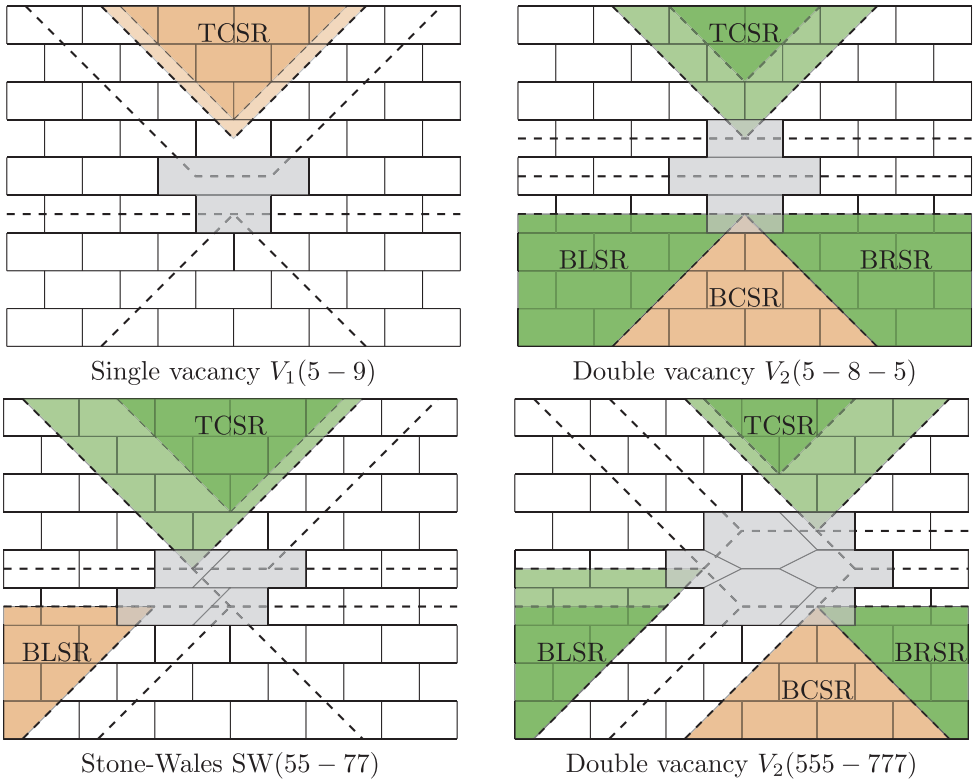

Figure 4. The sub-regions.

left by 2S1 units. This positions the detector at R3 and gives a value for S3. Note that R3 may be at the top or bottom of a vertical line depending on the value of S1.

4. *If R3 is in region A, then the break is SW, see Lemma 3.4.*
5. *If R3 is in region B move the detector $\frac{S3+1}{2}$ units from R3 to the right to reach R4 - which is at the top of a vertical line - and find the corresponding value S4.*
6. *If R4 is in region A then the break is $V_2(555-777)$ otherwise the break is $V_2(5-8-5)$, see Lemma 3.5.*

The following lemmas motivate the pertinent aspects of Algorithm 3.1 with detailed mathematical proofs.

Lemma 3.2. Let R1 be at the top of a vertical line. Moving directly up from R1 by *2S1* units ensures that R2 is in TCSR above the break. If TCSR is an A region then the break is a single vacancy.

Proof. In the following, $S1$ is split into three components.

1. $S1_H$: the number of horizontal steps from $R1$ to the break (not necessarily the same as the horizontal distance between $R1$ and the break, since to move up and down in the brick-wall grid, some horizontal steps are required to circumnavigate the bricks). The value $S1_H$ occurs twice in $S1$ as the path is closed and returns to $R1$.
2. $S1_V$: the number of vertical steps from $R1$ to the break. Again, this value occurs twice in $S1$ as the path is closed.
3. $S1_P$: the number of steps around an odd polygon in the break.

Let (x_1, y_1) be the coordinates of $R1$ then $(x_1, y_1 + 2S1)$ are the coordinates of $R2$. The lower boundary of the break is at least $S1_H$ units horizontally and $S1_V$ units vertically from $R1$. Moving $S1$ units up ensures that the point $(x_1, y_1 + S1) = (x_1, y_1 + 2(S1_H + S1_V) + S1_P)$ is above the break. Due to the shape of TCSR, if $R1$ is horizontally distant from the break, $S1$ further steps up will ensure that $(x_1, y_1 + 2S1)$ is in TCSR. There are sufficient steps to reach TCSR because any $S1_H$ steps are now converted into up steps and also, the $S1$ value includes 4 steps every time the path to the break includes two units up (because the brick structure does not allow a path to have two consecutive vertical steps).

Define (x_W, y_W) to be the lowest vertex of TCSR (in each of the four cases). Note that this vertex is one unit above the centre of the upper boundary of each break. An arbitrary point (x, y) is in TCSR if it satisfies the inequalities $y \geq x - x_W + y_W$ and $y \geq -x + x_W + y_W$, and from the reasoning above we know that $y_1 + S1 \geq y_W - 1$ (Figure 5).

Consider $R2$ with coordinates $(x_2, y_2) = (x_1, y_1 + 2S1)$ and show that they satisfy the above inequalities. If $R1$ is vertically in line with or to the right of the centre of the break then $y_1 \geq y_W - 1 - S1$ and $x_1 \leq x_W < x_W + S1 - 1$, thus $-x_1 \geq -x_W - S1 + 1$. Consequently,

$$\begin{aligned} y_2 - x_2 = y_1 + 2S1 - x_1 &\geq (y_W - 1 - S1) + 2S1 \\ &\quad + (-x_W - S1 + 1) = y_W - x_W. \end{aligned} \tag{1}$$

Similarly, if $R1$ is to the left of the centre of the break then $y_1 \geq y_W - 1 - S1$ and $x_W \leq x_1 + S1 - 1$, thus $x_1 \geq x_W - S1 + 1$. Hence,

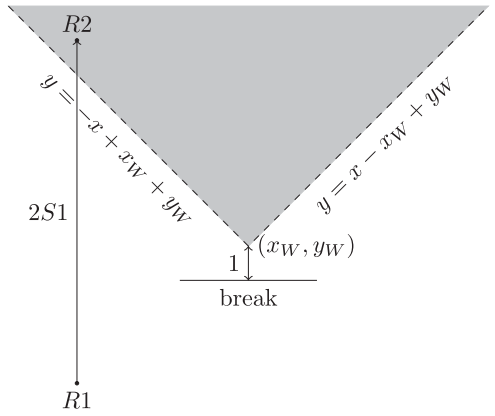

Figure 5. Position of *R2* in TCSR relative to *R1*.

$$y_2 + x_2 = y_1 + 2S1 + x_1 \geq (y_W - 1 - S1) + 2S1 + (x_W - S1 + 1) = y_W + x_W. \tag{2}$$

Since (1) and (2) hold, *R2* is in TCSR. As *R2* is an even number of units above *R1*, *R2* must be at the top of a vertical line and if $S2 \equiv 1(\text{mod}4)$ then *R2* is in region *A* (see Section 2) and the defect is a single vacancy. □

Remark 3.3. Note that it is enough to go up by $\frac{S1+7}{2}$ *units from R1, but it is simpler to use the above method and move up by* 2*S*1 *as it is more practical to apply and eliminates the need to consider several cases in the proof.*

In the next lemma we consider the scenario if *R2* (in Lemma 3.2) is in region *B*, i.e., $S2 \equiv 3(\text{mod}4)$.

Lemma 3.4. Let R2 be in region B. Moving down from R1 by $\frac{S1+1}{2}$ units and left by *2S1* units ensures that R3 is in BLSR. In addition, if R3 is in region A then the break is Stone-Wales.

Proof. We begin by defining the boundaries of BLSR in terms of inequalities.

Let (x_L, y_L) be the top right corner of BLSR, which is described as all the points (x, y) satisfying $x - x_L + y_L < y < y_L$.

If (x_1, y_1) are the coordinates of *R1* then $(x_3, y_3) = \left(x_1 - 2S1, y_1 - \frac{S1+1}{2}\right)$ are the coordinates of *R3*.

Recall that the lower boundary of the break is at least $S1_H$ units horizontally and $S1_V$ units vertically from *R1*. Moving $\frac{S1+1}{2}$ units down ensures that the point $(x_1, y_3) = (x_1, y_1 - (S1_H + S1_V) - \frac{S1_P+1}{2})$ is below the break. Note that $S1_V$ alone guarantees that we are in line with the break. Now $\frac{S1_P+1}{2} \geq 3$, and since the tallest break is 3 units high the point (x_1, y_3) is below the break. Therefore $y_3 < y_L$. Thus, after moving $\frac{S1+1}{2}$ units down the point (x_1, y_3) is at most $\frac{S1+1}{2} + S1_V$ units below the break and $y_3 > y_L - \frac{S1+1}{2} - S1_V - 1$.

The worst case scenario (i.e., the most steps needed for *R3* to be in BLSR) is when *R1* is below and to the right of the break. Then moving down by $\frac{S1+1}{2}$ units means that we are at most $S1_V + \frac{S1+1}{2} + 1$ units below y_L.

Moving left by $2S1 = 2(2S1_H + 2S1_V + S1_P)$ steps, results in *R3* being left of the break, because the *x*-coordinate of *R3* is less than $x_1 - S1_H - S1_P$. Note $S1_H$ steps take us at least to the right boundary of the break and then another $S1_P + 1$ steps take us to the left of x_L. Thus, $x_3 < x_L - 4S1_V - 3S1_H - (S1_P - 1)$. Combining

$$\begin{aligned} -x_3 &> -x_L + 4S1_V + 3S1_H + S1_P - 1 \\ &= -x_L + 2S1_V + 2S1_H - 1 + \left(\frac{S1+1}{2} + S1_V\right) + \frac{S1_P - 1}{2} \end{aligned} \tag{3}$$

with

$$y_3 > y_L - \frac{S1+1}{2} - S1_V - 1 \tag{4}$$

yields

$$\begin{aligned} y_3 - x_3 &> y_L - \frac{S1+1}{2} - S1_V - 1 - x_L + 2S1_V + 2S1_H - 1 \\ &+ \left(\frac{S1+1}{2} + S1_V\right) + \frac{S1_P - 1}{2} \\ &= y_L - x_L + 2S1_V + 2S1_H + \frac{S1_P - 5}{2} > y_L - x_L. \end{aligned} \tag{5}$$

Therefore (x_3, y_3) satisfies the inequalities $x_3 - x_L + y_L < y_3 < y_L$ and thus *R3* lies in BLSR. Note that *R3* can be at the top or the bottom of a vertical line as $\frac{S1+1}{2}$ can be odd or even. Thus we will need to apply one of the statements from Section 2.

If $S1 \equiv 1(\text{mod}4)$ (even number of steps down, i.e. *R3* at the top of a vertical line) and $S3 \equiv 1(\text{mod}4)$ then *R3* is in region *A*. If $S1 \equiv 3(\text{mod}4)$ (odd number, *R3* at the bottom of a vertical line) and $S3 \equiv 3(\text{mod}4)$ then *R3* is in region *A*. If *R3* is in region *A*, then the break is a Stone-Wales defect. □

In the following lemma we consider the case when *R3* (in Lemma 3.4) is in region *B* and then distinguish between the two DV breaks.

Lemma 3.5. If BLSR is a B region, moving $\frac{S3+1}{2}$ to the right from R3 we reach R4 with S4. If R4 is in region A then the break is $V_2(555 - 777)$ otherwise it is in region B and the break is $V_2(5 - 8 - 5)$.

Remark 3.6. If R3 is at the top of a vertical line, then $S3 \equiv 3(\text{mod}4)$ *because R3 is in a B region. Hence* $\frac{S3+1}{2}$ *is even and thus R4 is also at the top of a vertical line.*

Similarly, if R3 is at the bottom of a vertical line, then $S3 \equiv 1(\text{mod}4)$ *because again R3 is in a B region. Hence* $\frac{S3+1}{2}$ *is odd and thus R4 is at the top of a vertical line.*

Proof of Lemma 3.5. We provide the proof for *R3* at the top of a vertical line and omit the analogous proof for *R3* at the bottom of a vertical line which follows similar reasoning.

We use an inductive argument to explain why moving $\frac{S3+1}{2}$ steps to the right will take us to the left-most vertices of BRSR (a *B* region) in the case of $V_2(5 - 8 - 5)$ and the right-most vertices of BCSR (an *A* region) in the case of $V_2(555 - 777)$.

The base case of the induction is as follows. For $V_2(5-8-5)$, if $R3$ is at the top of a vertical line in BLSR, the smallest possible value of $S3$ is $S3_0 = 7$. Let us denote this point by $R3_0 = (x_0, y_0)$. In this case, the position of $R4_0 = (x_0 + 4, y_0)$ is $\frac{S3_0+1}{2} = 4$ vertices to the right of $R3_0$ and at the top left-most vertex of BRSR (neighbouring the left boundary).

For the induction hypothesis, assume that moving $\frac{S3_k+1}{2}$ steps to the right from a right-most vertex (x_k, y_k) in BLSR at the top of a vertical line will mean that $R4_k = \left(x_k + \frac{S3_k+1}{2}, y_k\right)$ is at the top of a vertical line in BRSR (next to the left boundary).

Now for the induction step, we move right by $\frac{S3_{k+1}+1}{2} = \frac{S3_k+5}{2}$ units from the point $R3_{k+1} = (x_k - 1, y_k - 1)$ to $R4_{k+1}$. Note that $S3_{k+1}$ is 4 units more than $S3_k$, since there are two more units in the path and they are traversed twice. Thus the horizontal distance between $R3_{k+1}$ and $R4_{k+1}$ is two more units than the distance between $R3_k$ and $R4_k$.

Hence $R4_{k+1}$ is one unit to the right and one unit down from $R4_k$ which is at the top of a vertical line in BRSR (adjacent to the left boundary) and it has the following coordinates $R4_{k+1} = \left(x_k - 1 + \frac{S3_k+5}{2}, y_k - 1\right) = \left(x_k + \frac{S3_k+1}{2} + 1, y_k - 1\right)$. Thus we have shown by inductive reasoning that if $R3$ is any point at the top of a vertical line and adjacent to the right boundary of BLSR, then $R4$ will be adjacent to the left boundary of BRSR for a $V_2(5-8-5)$ defect.

Let us assume that we are at the top of a vertical line $2n$ units to the left from $R3_k$ (i.e., at a general point in BLSR - not necessarily bordering the boundary with BCSR). Then the length of the shortest closed path is $S3_k + 4n$. If $R4_k$ is $\frac{S3_k+4n+1}{2} = \frac{S3_k+1}{2} + 2n$ units to the right of $R3_k$ then it is at the top of a vertical line in BRSR adjacent to the boundary with BCSR.

For the case of $V_2(555-777)$ the inductive proof is similar to that of $V_2(5-8-5)$. The only differences are the base case and that $R4$ is $\frac{S3+1}{2}$ steps to the right of $R3$ and it is the right-most vertex of BCSR adjacent to the boundary with BRSR (on the same horizontal level as $R3$).

More specifically, the base case for $V_2(555-777)$ is as follows. If $R3$ is at the top of a vertical line in BLSR then the smallest possible value of $S3$ is $S3_0 = 11$. We denote this point by $R3_0 = (x_0, y_0)$. Now $R4_0 = (x_0 + 6, y_0)$ is $\frac{S3_0+1}{2} = 6$ units to the right of $R3_0$ and is at the top (right-most) vertex of BCSR.

Thus, if $R4$ is in a B region then the break is $V_2(5-8-5)$ and if $R4$ is in an A region then the break is $V_2(555-777)$. □

In conclusion, we have provided an algorithm to identify which one of the four breaks listed in this paper occurs in a graphene lattice. Moreover, once the type of break has been established, the exact position of the break can be determined using the results in.[17–19]

Disclosure statement

No potential conflict of interest was reported by the authors.

Funding

This work was supported by the National Research Foundation of South Africa under grant no.s 89147 and 103530.

ORCID

Margaret Archibald http://orcid.org/0000-0001-5635-6733
Sonja Currie http://orcid.org/0000-0003-2190-8862
Marlena Nowaczyk http://orcid.org/0000-0003-3657-1609

References

[1] Liu, L.; Qing, M.; Wang, Y.; Chen, S. Defects in Graphene: Generation, Healing, and Their Effects on the Properties of Graphene: A Review. *J. Mater. Sci. Technol.* **2015**, *31*, 599–606. DOI: 10.1016/j.jmst.2014.11.019.

[2] Banhart, F.; Kotakoski, J.; Krasheninnikov, A. V. Structual Defects in Graphene. *Am. Chem. Soc.* **2011**, *5*, 26–41. DOI: 10.1021/nn102598m.

[3] Meyer, J. C.; Kisielowski, C.; Erni, R.; Rossell, M. D.; Crommie, M. F.; Zettl, A. Direct Imaging of Lattice Atoms and Topological Defects in Graphene Membranes. *Nano Lett.* **2008**, *8*, 3582–3586. DOI: 10.1021/nl801386m.

[4] Kotakoski, J.; Krasheninnikov, A. V.; Nordlund, K. Energetics, Structure, and Long-Range Interaction of Vacancy-Type Defects in Carbon Nanotubes: Atomistic Simulations. *Phys. Rev. B* **2006**, *74*, 245420. DOI: 10.1103/PhysRevB.74.245420.

[5] Liu, L.; Chen, S. Geometries and Electronic States of Divacancy Defect in Finite-Size Hexagonal Graphene Flakes. *J. Chem.* **2017**, *2017*, 1–7. DOI: 10.1155/2017/8491264.

[6] Ori, O.; Putz, M. V. Bondonic Characterization of Extended Nanosystems: Application to Graphene's Nanoribbons. *Chem. Phys. Lett.* **2012**, *548*, 95–100. DOI: 10.1016/j.cplett.2012.08.019.

[7] Ori, O.; Putz, M. V. Bondonic Effects in Group-IV Honeycomb Nanoribbons with Stone-Wales Topological Defects. *Molecules* **2014**, *19*, 4157–4188. DOI: 10.3390/molecules19044157.

[8] Ori, O.; Cataldo, F.; Putz, M. V. Topological Anisotropy of Stone-Wales Waves in Graphenic Fragments. *Int. J. Mol. Sci.* **2011**, *12*, 7934–7949. DOI: 10.3390/ijms12117934.

[9] Ori, O.; Putz, M. V. Isomeric Formation of 5—8—5 Defects in Graphenic Systems. *Nanotubes Carbon Nanostruct.* **2014**, *22*, 887–900. DOI: 10.1080/1536383X.2012.749454.

[10] Wang, Y.; Yang, C.; Cheng, Y.; Zhang, Y. A Molecular Dynamics Study on Thermal and Mechanical Properties of Graphene–Paraffin Nanocomposites. *RSC Adv.* **2015**, *5*, 82638–82644. DOI: 10.1039/C5RA12028D.

[11] Ni, B.; Zhang, T.; Li, J.; Li, X.; Gao, H. *Topological Design of Graphene, Volume II: Handbook of Graphene Set: Physics, Chemistry, and Biology*, Wiley Online Library, **2019**; pp 1–44. DOI: 10.1002/9781119468455.ch19.

[12] Sh. Sabirov, D.; Ori, O. Skeletal Rearrangements of the C_{240} Fullerene: Efficient Topological Descriptors for Monitoring Stone–Wales Transformations. *Mathematics* **2020**, *8*, 968. DOI: 10.3390/math8060968.

[13] Zhang, T.; Li, X.; Gao, H. Defects Controlled Wrinkling and Topological Design in Graphene. *J. Mech. Phys. Solids* **2014**, *67*, 2–13. DOI: 10.1016/j.jmps.2014.02.005.

[14] Kuchment, P. Graph Models for Waves in Thin Structures. *Waves Random Media* **2002**, *12*, R1–R24. DOI: 10.1088/0959-7174/12/4/201.

[15] Kurasov, P.; Nowaczyk, M. Inverse Spectral Problem for Quantum Graphs. *J. Phys. A: Math. Gen.* **2005**, *38*, 4901–4915. DOI: 10.1088/0305-4470/38/22/014.

[16] Wakabayashi, K.; Sasaki, K.; Nakanishi, T.; Enoki, T. Electronic States of Graphene Nanoribbons and Analytical Solutions. *Sci. Technol. Adv. Mater.* **2010**, *11*, 054504. DOI: 10.1088/1468-6996/11/5/054504.

[17] Archibald, M.; Currie, S.; Nowaczyk, M. Finding the Hole in a Wall. *J. Math. Chem.* **2020**, *58*, 2313–2323. DOI: 10.1007/s10910-020-01178-3.

[18] Archibald, M.; Currie, S.; Nowaczyk, M. Locating a Double Vacancy or Stone-Wales Point Defect on a Hexagonal Quantum Grid. *J. Math. Chem.* **2022**, *60*, 862–873. DOI: 10.1007/s10910-022-01337-8.

[19] Archibald, M.; Currie, S.; Nowaczyk, M. Finding the $V_2(555-777)$ Double Vacancy Defect in Graphene Using Rotational Symmetry. *Iran. J. Math. Chem.* **2023**, *14*, 55–64. DOI: 10.22052/ijmc.2023.247422.1653.

[20] Montambaux, G. Artificial Graphenes: Dirac Matter beyond Condensed Matter. *C. R. Phys. Elsevier Masson* **2018**, *19*, 285–305. DOI: 10.1016/j.crhy.2018.10.010.